loss tangent," *IEEE Trans. Instrum. Meas.*, vol. IM-17, pp. 413–417, 1968.
[42] R. G. Jones, "The measurement of dielectric anisotropy using a microwave open resonator," *J. Phys. D. Appl. Phys.*, vol. 9, pp. 819–827, 1976.
[43] K. H. Breeden and J. B. Langley, "Fabry–Perot cavity for dielectric measurements," *Rev. Sci. Inst.*, vol. 40, pp. 1162–1163, 1969.
[44] R. J. Cook and R. G. Jones, "Precise dielectric measurement techniques for the frequency range 10 GHz to 150 GHz," in *Proc. 8th Eur. Microwave Conf. Paris* (Sevenoaks: Microwave Exhibitions and Publishers), 1978, pp. 528–532.
[45] R. H. Stolen, "Far infrared absorption in high resistivity GaAs," *Appl. Phys. Letts.*, vol. 15, pp. 74–75, July 1969.

Mohammed Nurul Afsar (SM'81) received the Bachelor of Science (B.Sc.) degree and the Master of Science (M.Sc) degree in physics from the University of Dacca, presently in Bangladesh, and the M.Sc.E.E. degree in microwaves and quantum electronics, the University College London post-graduate diploma in microwave engineering, and the Ph.D. degree in experimental physics from the University of London, England.

At the University College of the University of London, his research field was on tropospheric propagation. From 1972 until 1978, he worked at the prestigious National Physical Laboratory (NPL) of England, in the Division of Electrical Science, where he was responsible for the development of millimeter- and submillimeter-wave (60 GHz–18 THz) measurement techniques and instrumentation on solids, liquids, and gases involving application of methods such as Fourier-transform spectroscopy and laser spectroscopy. He has also made theoretical studies of various systems such as water, alcohol, and hydrogen bonded molecules, critical mixtures, polymers, semiconductors, and common gases and pollutants. He was also responsible for the European Economic Community (EEC) funded Inter-European project on standard reference material. He was awarded the 1977 Duddell Premium (prize) by the Institution of Electrical Engineers, London (IEE), for one of his outstanding publications. In 1978, he joined the Massachusetts Institute of Technology (MIT), Cambridge, where he is a Senior Scientist and Principal Investigator of several research projects. His main line of research at the MIT National Magnet Laboratory is millimeter- and submillimeter-wave techniques and precision measurements and the theoretical study of complex refractive index and dielectric permittivity, and magnetic permeability of condensed materials and window design for high-power gyrotron source and magnetooptical study and impurity characterization of gallium arsenide, indium phosphide, and ternary and quaternary compound semiconductors. He is one of the organizers of the annual International Conference on Infrared and Millimeter Waves. In September 1984, he took a new position as full Professor, Department of Electrical Engineering, at the City College of the City University of New York and Graduate School of the City University of New York. He has published over one hundred papers, including several book chapters, and has established himself as a world expert in the microwave, millimeter-wave, micro-electronics fields. He routinely presents invited talks at many international conferences..

Dr. Afsar is a Chartered Engineer, England, and a Member of the Institution of Electrical Engineers, London (IEE), and a Member of the Institute of Physics, London, and a member of the American Physical Society.

Computed Modal Field Distributions for Isolated Dielectric Resonators

DARKO KAJFEZ, SENIOR MEMBER, IEEE, ALLEN W. GLISSON, MEMBER, IEEE, AND JOSEPH JAMES, STUDENT MEMBER, IEEE

Abstract—**Electric- and magnetic-field patterns for five of the lowest resonant modes in cylindrical dielectric resonators are displayed in various planes of intersection. The computational procedure is based on a method-of-moments solution of the surface integral equation for bodies of revolution. Improvement of the numerical stability through the normalization of the matrix is discussed, and an algorithm for the evaluation of the modal field components is described.**

I. Introduction

THE resonant frequencies and the Q factors of various modes in isolated dielectric resonators can be accurately computed by using the surface integral equation formulation for bodies of revolution as described in [1]. In this paper, we present results for the computed field distributions of several modes of an isolated resonator which were obtained by applying this formulation. In the first section of the paper, a normalization procedure used in [1] is described. Numerical implementation of the integral equation approach may lead to numerical instabilities when higher order modes are studied if the moment matrix is not adequately normalized. It is shown that a straightforward normalization can significantly improve the condition number of the matrix [2], and consequently remove or reduce the numerical difficulties.

Traditional applications of the method of moments to problems involving perfectly conducting bodies have been either an E-field or an H-field integral equation [3], [4]. In either case, all the components of the unknown column vector are automatically expressed in the same physical units for most structures so that the normalization of the matrix is not an issue. The integral equation utilized here,

Manuscript received May 3, 1984; revised July 25, 1984. This material is based upon work supported by the National Science Foundation under Grant ECS-8304442.

D. Kajfez and A. W. Glisson are with the Department of Electrical Engineering, University of Mississippi, University, MS 38677.
J. James is with South Carolina State College, Orangeburg, SC 29117.

0018-9480/84/1200-1609$01.00 ©1984 IEEE

however, is of the combined-field type [5], [6], in which both the electric and the magnetic equivalent currents appear as unknowns. In such situations, and when different types of basis functions are used for different components of current, the matrix should be normalized in such a way that all the components of the column vectors on both sides of the matrix equation are reduced to the same physical units.

A convenient computational procedure for evaluating electric- and magnetic-field distributions in and around the dielectric resonator is described in the second section. It is shown that the components of the modal field vectors can be computed using a slight modification of the existing algorithm for computation of the matrix elements in the method-of-moments procedure.

In the last part of the paper, the computed field distributions for various resonant modes are graphically displayed. A detailed knowledge of the orientation of the electric and the magnetic field around the resonator should be very useful in designing the coupling circuits for particular modes, as well as in designing the traps for undesirable modes. Only the field distributions of the rotationally symmetric $TE_{01\delta}$ and $TM_{01\delta}$ modes have been previously shown in the literature on dielectric resonators [7], [8].

II. Matrix Normalization

The two coupled integral equations which serve as a starting point in the solution procedure utilized here are obtained from the boundary condition that both the tangential electric and the tangential magnetic fields are continuous at the surface of the dielectric resonator. When the unknown equivalent surface currents are expanded in pulse basis functions and the integral equations are tested in the manner described in [1], a matrix equation of the following form is obtained:

$$\begin{pmatrix} \underset{\sim}{Z}_{tt} & \underset{\sim}{Z}_{t\phi} & \underset{\sim}{\Gamma}_{tt} & \underset{\sim}{\Gamma}_{t\phi} \\ \underset{\sim}{Z}_{\phi t} & \underset{\sim}{Z}_{\phi\phi} & \underset{\sim}{\Gamma}_{\phi t} & \underset{\sim}{\Gamma}_{\phi\phi} \\ -\underset{\sim}{\Gamma}_{tt} & -\underset{\sim}{\Gamma}_{t\phi} & \underset{\sim}{Y}_{tt} & \underset{\sim}{Y}_{t\phi} \\ -\underset{\sim}{\Gamma}_{\phi t} & -\underset{\sim}{\Gamma}_{\phi\phi} & \underset{\sim}{Y}_{\phi t} & \underset{\sim}{Y}_{\phi\phi} \end{pmatrix} \begin{pmatrix} |I_t\rangle \\ |J_\phi\rangle \\ |K_t\rangle \\ |M_\phi\rangle \end{pmatrix} = \begin{pmatrix} |E_t^i\rangle \\ |E_\phi^i\rangle \\ |H_t^i\rangle \\ |H_\phi^i\rangle \end{pmatrix}. \quad (1)$$

Subscripts ϕ and t in (1) denote vector components in the azimuthal direction and in the direction along the generating curve for the body of revolution, respectively. Fig. 1 illustrates the orientation of the components of equivalent electric surface currents J_t and J_ϕ on various parts of the dielectric resonator of cylindrical shape.

The integrals appearing in the evaluation of elements of the moment matrix are simplified if one multiplies the J_t and M_t components of the unknown equivalent currents by the factor $2\pi\rho$, where ρ is the radial distance to the current source in a cylindrical system of coordinates, and then treats this product as the unknown quantity in the equation. By doing this, the physical dimension of these two variables is changed from current density to current. Thus, the t-components of the electric and magnetic currents appearing in (1) are denoted I_t and K_t. The column

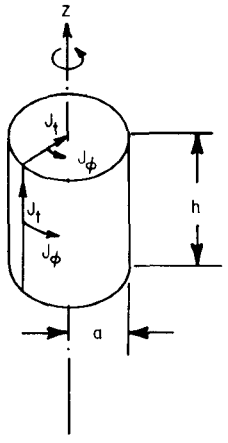

Fig. 1. Orientation of equivalent currents on surface of dielectric resonator.

vector of the unknown equivalent currents (and current densities) is partitioned in four column vectors $|I_t\rangle$, $|J_\phi\rangle$, $|K_t\rangle$, and $|M_\phi\rangle$.

The homogeneous solution of the matrix equation (1) yields the numerical values of the natural frequencies on the complex plane which belong to various resonant modes. However, when the number of points N is gradually increased in order to study the numerical convergence of the method, one may encounter numerical instabilities in computing the equivalent currents of some resonant modes. This indicates that the matrix in (1) becomes ill-conditioned for large N.

The reason for the ill-conditioning can be traced to the fact that the individual components of both column vectors appearing in (1) are expressed in mixed physical units. For instance, I_t is given in amperes, J_ϕ in amperes per meter, K_t in volts, and M_ϕ in volts per meter. In order to correct this situation, I_t and J_ϕ are both multiplied by the intrinsic impedance η_r of the dielectric material

$$\eta_r = \frac{120\pi}{\sqrt{\epsilon_r}}. \quad (2)$$

In addition, I_t is divided by $2\pi a$, the circumference of the resonator. The new normalized column vectors, denoted by primed symbols, are then

$$|J_t'\rangle = \frac{\eta_r}{2\pi a}|I_t\rangle \quad (3)$$

$$|J_\phi'\rangle = \eta_r|J_\phi\rangle. \quad (4)$$

We note that the new vector $|J_t'\rangle$ has units of current density, but it is not the actual equivalent surface current density because of the factor ρ/a. The vector $|M_\phi\rangle$ is left unchanged, and the vector $|K_t\rangle$ is normalized by dividing by $2\pi a$

$$|M_t'\rangle = \frac{1}{2\pi a}|K_t\rangle. \quad (5)$$

The new primed symbols are now all expressed in the same physical units, namely volts/meter. This change of variables requires that the corresponding parts of the partitioned matrix in (1) be divided (or multiplied) by the same

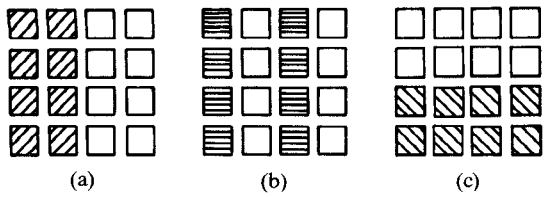

Fig. 2. Matrix areas affected by normalization: (a) division by η_r, (b) multiplication by $2\pi a$, and (c) multiplication by η_0.

factors. Therefore, the first two block-columns of the matrix must be divided by η_r as indicated in Fig. 2(a). The first and the third block-columns must also be multiplied by $2\pi a$ as indicated in Fig. 2(b).

To bring the right-hand side of (1) to the same physical units, all the magnetic-field quantities are multiplied with the free-space intrinsic impedance η_0. Consequently, the third and the fourth block-rows of the matrix must be multiplied by the same factor as shown in Fig. 2(c).

The condition number based on the infinite norm [2] has been computed before and after the normalization indicated above. For the mode $HEM_{12\delta}$ with 27 points on the body (resulting in a 102×102 matrix), the matrix condition number was reduced by a factor 10^6. The dielectric resonator dimensions are $a = 5.25$ mm and $h = 4.6$ mm, and the relative dielectric constant is $\epsilon_r = 38$.

The effect of bringing all the elements of the current vector to the same units can be seen in Fig. 3. In this figure, the values of the individual currents are plotted in order of appearance in the column vector. There are a total of 102 current values plotted. In Fig. 3(a), the equivalent currents computed without matrix normalization are plotted, and in Fig. 3(b), the currents computed with normalization are plotted. One can clearly see that the unnormalized currents are so dissimilar in magnitude that, for instance, the equivalent current I_t is not even visible in the illustration. After normalization, all the equivalent current densities are of the same order of magnitude, as can be seen in Fig. 3(b).

III. Computation of Fields

Once a resonant frequency of the dielectric resonator has been determined, the modal equivalent surface currents can be computed from (1) within a multiplicative constant. A convenient numerical procedure for doing this is Gaussian elimination. The resulting electric and magnetic equivalent surface currents on the elementary "bands" on the resonator surface can be utilized to compute the electric and magnetic fields everywhere in space. However, the vector summation of the field contributions for various observation points inside and around the resonator requires a considerable additional programming effort. This work can be circumvented by utilizing the information already available in the subroutine which computes the elements of the matrix on the left-hand side of (1).

A convenient procedure can be developed for computing the fields if one notes that the surface integral equation approach comprises a difference of the two fields of interest at the resonator surface since the equations are of the

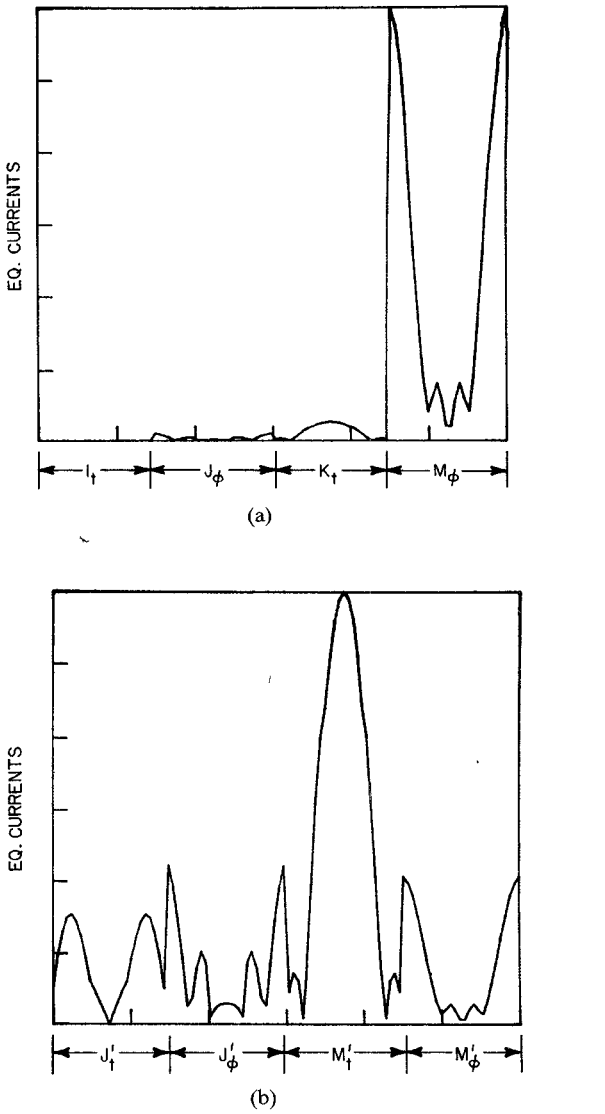

Fig. 3. Magnitude of modal equivalent currents for $HEM_{12\delta}$ mode: (a) for unnormalized matrix, and (b) for normalized matrix.

form

$$[\boldsymbol{E}^s(\boldsymbol{J},\boldsymbol{M}) - \boldsymbol{E}(-\boldsymbol{J},-\boldsymbol{M})]_{\tan} = \boldsymbol{E}^{\text{inc}}_{\tan} \tag{6}$$

$$[\boldsymbol{H}^s(\boldsymbol{J},\boldsymbol{M}) - \boldsymbol{H}(-\boldsymbol{J},-\boldsymbol{M})]_{\tan} = \boldsymbol{H}^{\text{inc}}_{\tan} \tag{7}$$

where $(\boldsymbol{E}^s, \boldsymbol{H}^s)$ and $(\boldsymbol{E}, \boldsymbol{H})$ are the fields evaluated just outside and just inside the resonator surface, respectively. In particular, a single element of the moment matrix represents the difference in two field components at some point in space due to two different unit current sources (e.g., from basis functions for $\boldsymbol{J}$ and $-\boldsymbol{J}$) located at another point in space, but which radiate in different homogeneous media. The two radiated fields appearing in (6) and (7) are computed individually, and hence the correct field in either region can be computed by retaining only the appropriate terms in the moment-matrix calculation. This is easily accomplished by retaining only the set of potentials where the medium parameters are those of the medium in which the field is desired.

To compute the fields, therefore, we first specify the generating arc for a phantom surface on which we wish to

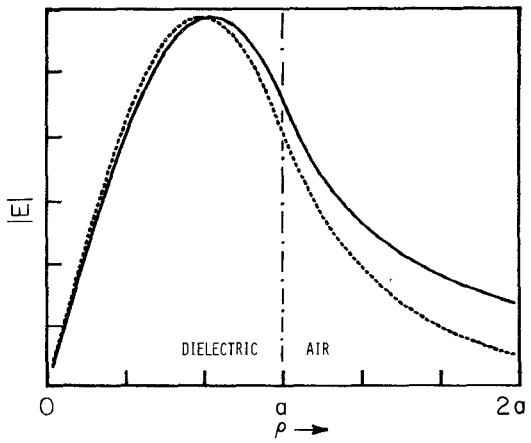

Fig. 4. Solid line: electric field versus radial distance, isolated resonator, mode $TE_{01\delta}$. Broken line: dielectric rod resonator TE_{011} between parallel magnetic walls. Dimensions: $a = 5.25$ mm, $h = 4.6$ mm; dielectric constant: $\epsilon_r = 38$.

know the tangential fields. The fields tangential to this surface due to unit sources on the resonator surface are next computed using a modified version of the moment-matrix routine which includes only the potentials involving the Green's function of the medium in which the field is to be evaluated. The resulting matrix is multiplied by the previously computed modal current solution to obtain the tangential fields on the generating arc of the phantom surface. The fields so computed are actually weighted averages, since (6) and (7) were "tested" as described in [1] to obtain expressions for the moment-matrix elements. The appropriate values for the fields are easily obtained, however, by dividing by the length of the phantom surface subdomain at the observation point. Fields anywhere on the phantom surface are obtained by including the appropriate $\cos(m\phi)$ or $\sin(m\phi)$ behavior, where m is the azimuthal mode number.

For the mode $TE_{01\delta}$, field distributions obtained via this procedure have been compared with the theoretical distribution for a dielectric-rod waveguide for which the solution is available in terms of Bessel functions [9]. One observes in Fig. 4 that the agreement is quite good inside the resonator. The field of the isolated resonator, however, decays more slowly than does the field for a resonant section of the dielectric-rod waveguide terminated by two parallel magnetic walls. This behavior is to be expected since the magnetic walls form a cutoff waveguide in the radial direction (see, e.g., [10, fig. 5]).

IV. Catalog of Field Patterns

In this section, we present a catalog of electric- and magnetic-field patterns for several low-order resonant modes in isolated dielectric resonators. The computed vector field $\boldsymbol{F}$ (electric or magnetic field) for a particular mode is an exponentially decaying oscillation. Even if the decaying nature of the field is ignored, it is difficult to graphically represent the spatial distribution of the magnitude and the phase of $\boldsymbol{F}$. Therefore, we display the instantaneous values of the vector

$$\mathrm{Re}\left(\boldsymbol{F}e^{j\omega_{mnp}t}\right)$$

at several instants of time, like

$$\omega_{mnp}t = 0, \frac{\pi}{4}, \frac{\pi}{2}, \text{ etc.}$$

TABLE I
Resonant Frequencies and Q Factors of the Five Lowest Modes

Mode	f_{res} (GHz)	Q
$TE_{01\delta}$	4.829	45.8
$TM_{01\delta}$	7.524	76.8
$HEM_{11\delta}$	6.333	30.7
$HEM_{12\delta}$	6.638	52.1
$HEM_{21\delta}$	7.752	327.1

In the above, we use ω_{mnp} to represent only the imaginary part of the complex natural frequency of the mode (m, n, p). A computer-generated graphical display is used to show the field orientation at equidistant points as well as to provide some relative amplitude information. The plane containing the z axis (axis of rotation) is referred to as the meridian plane, and the plane perpendicular to it, passing through the center of the resonator, is referred to as the equatorial plane. All the plots are computed for a resonator having the dimensions $a = 5.25$ mm and $h = 4.6$ mm, and which is made of material with $\epsilon_r = 38$. The resonant frequencies and the Q factors (due to radiation) are listed in Table I. When compared with the results presented in [1], it is noticed that the resonant frequencies are almost identical, but some of the Q factors differ by as much as 12 percent. The results presented here for the Q factors are believed to be more accurate than those in [1] because a larger number of points has been utilized to model the generating arc of the resonator.

Fig. 5 shows the electric field of the mode $TE_{01\delta}$ in the equatorial plane at the moment $\omega_{mnp}t = 0$. In this and in subsequent illustrations, double arrows indicate the area within which the field is less than 3 dB below the maximum, while the longer lines indicate a level between 3 and 10 dB below the maximum, and the shorter lines indicate a level between 10 and 20 dB below the maximum. When the transverse field is more than 20 dB below the maximum value of the field, the points are left blank. The magnetic field of the mode $TE_{01\delta}$ in the meridian plane is shown in Fig. 6. The magnetic field is perpendicular to the field shown in Fig. 5, and its maximum occurs one-quarter period later in time. In general, all the magnetic-field patterns are in time quadrature with all the electric-field patterns. Therefore, this fact will not be further indicated in the remaining illustrations.

The magnetic and electric field of the $TM_{01\delta}$ mode can be seen in Figs. 7 and 8 in the equatorial and meridian planes, respectively. The magnetic field of this mode is well

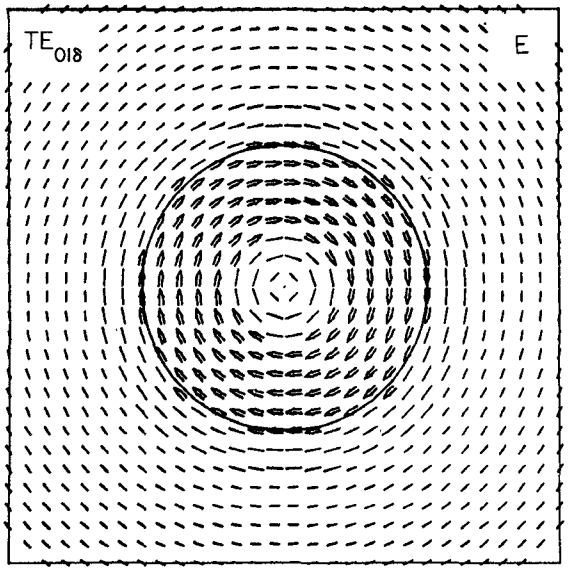

Fig. 5. $TE_{01\delta}$ mode, E-field in equatorial plane, $\omega t = 0$.

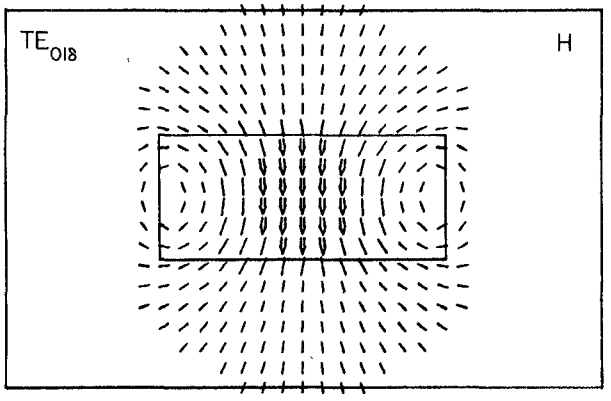

Fig. 6. $TE_{01\delta}$ mode, H-field in meridian plane, $\omega t = \pi/2$.

contained within the resonator, whereas the outside electric field is relatively strong near the top and bottom faces of the resonator. If strong coupling to an external circuit is desired, a short capacitive probe, directed along the axis of rotation, should be well-suited for coupling to this mode.

The remaining three resonant modes displayed here are hybrid electromagnetic modes (HEM) [10] with respect to the axis of rotation. Each of these modes has a degeneracy in the sense that, as a function of the angle ϕ, it can acquire either a $\cos(m\phi)$ or a $\sin(m\phi)$ dependence. For this reason, the angular reference $\phi = 0$ is indicated to specify the orientation of various field patterns with respect to each other.

The hybrid mode with the lowest resonant frequency is $HEM_{11\delta}$ shown in Figs. 9 through 12. As mentioned in [1], it was not possible to observe this mode experimentally in the free-space simulated environment. Table I shows that the Q factor of this mode is lowest of all the modes, which makes it very difficult to achieve sufficient coupling to the coaxial cable leading to the observation instrument. This mode has been recently utilized by Long *et al.* [11] in the so-called resonant cylindrical dielectric cavity antenna.

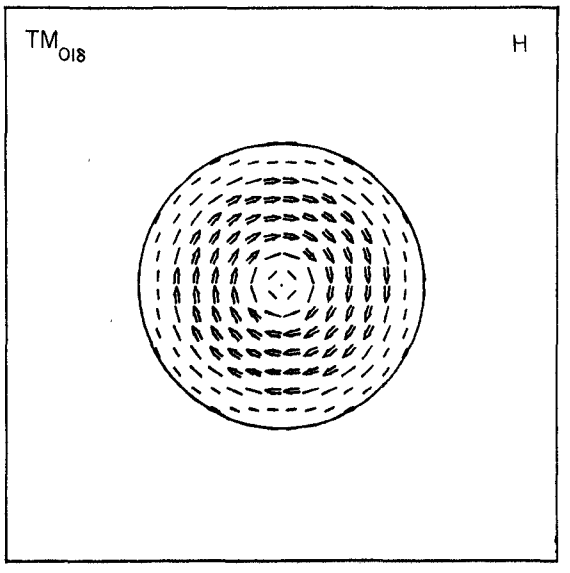

Fig. 7. $TM_{01\delta}$ mode, H-field in equatorial plane.

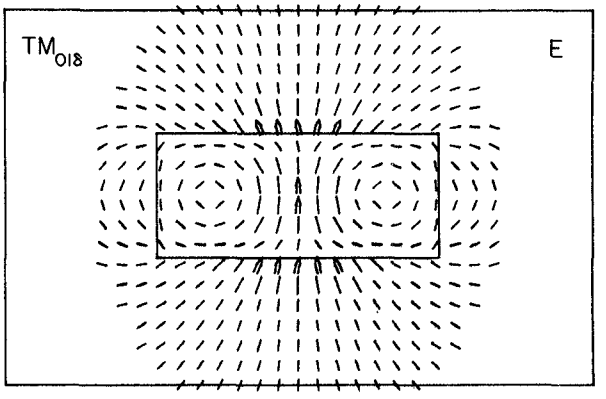

Fig. 8. $TM_{01\delta}$ mode, E-field in meridian plane.

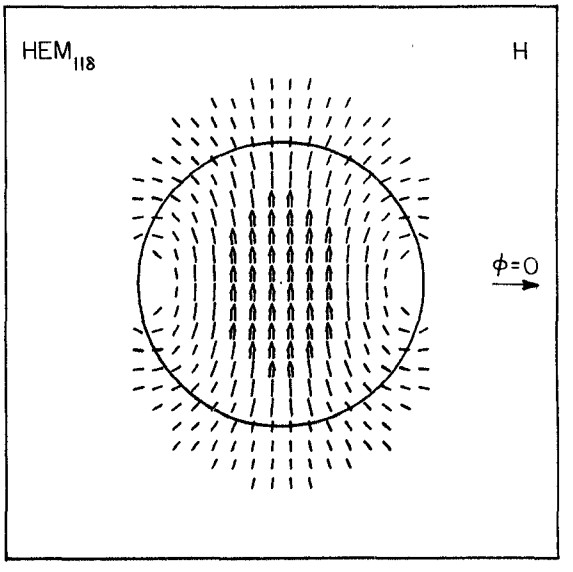

Fig. 9. $HEM_{11\delta}$ mode, H-field in equatorial plane.

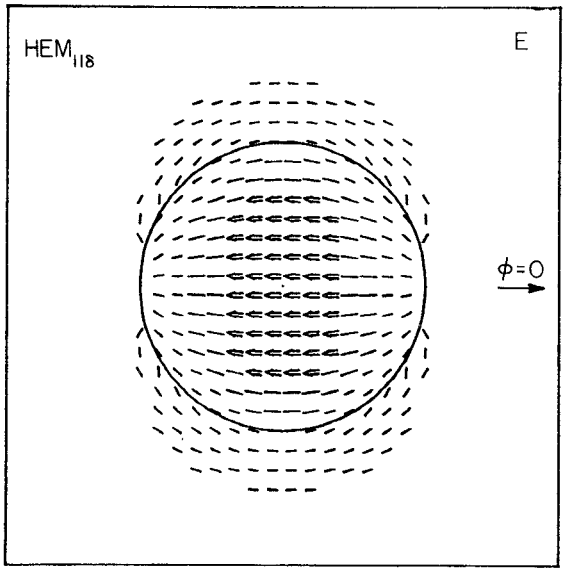

Fig. 10. $HEM_{11\delta}$ mode, E-field in plane parallel to and offset from equatorial plane by 2.15 mm.

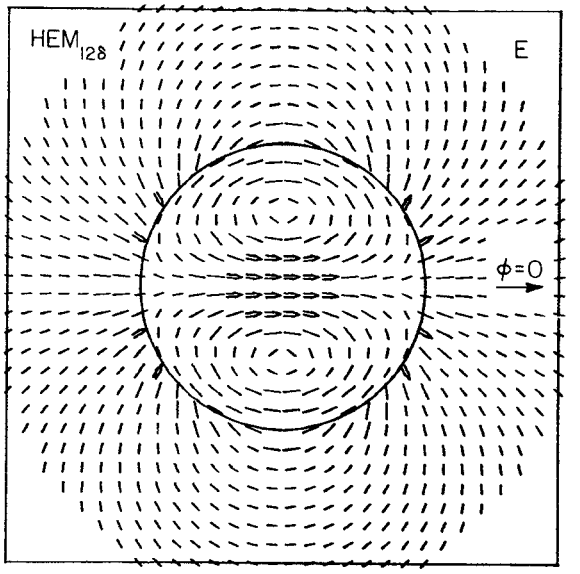

Fig. 13. $HEM_{12\delta}$ mode, E-field in equatorial plane.

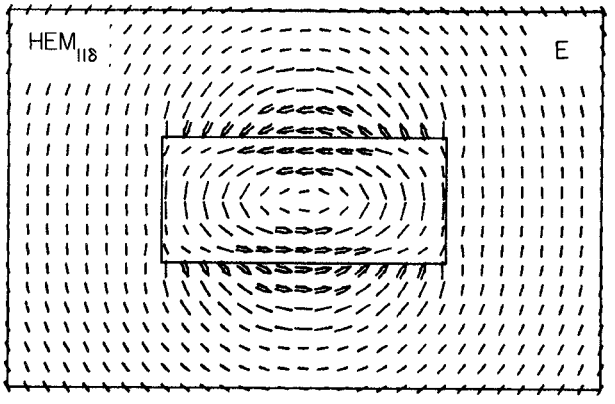

Fig. 11. $HEM_{11\delta}$ mode, E-field in meridian plane $\phi = 0$.

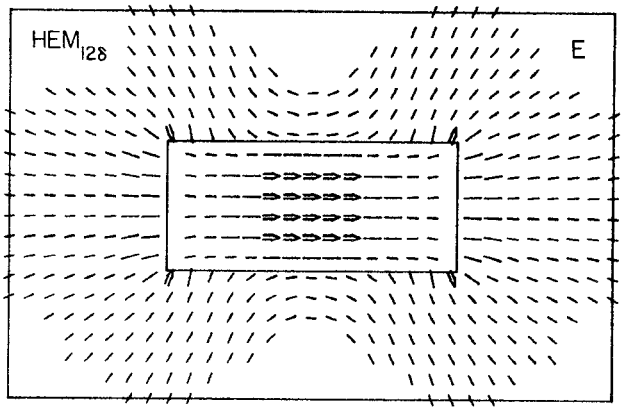

Fig. 14. $HEM_{12\delta}$ mode, E-field in meridian plane $\phi = 0$.

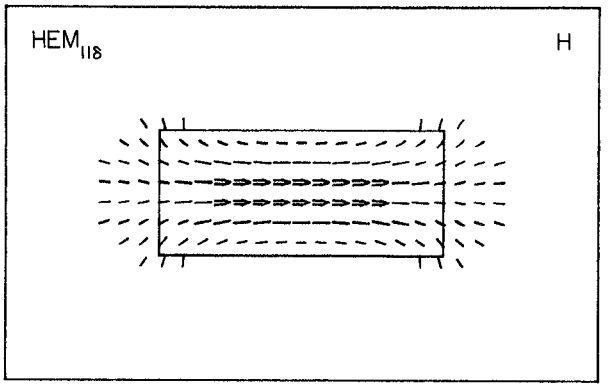

Fig. 12. $HEM_{11\delta}$ mode, H-field in meridian plane $\phi = \pi/2$.

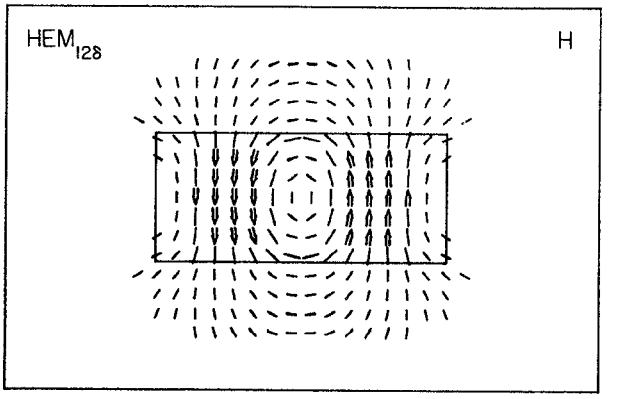

Fig. 15. $HEM_{12\delta}$ mode, H-field in meridian plane $\phi = \pi/2$.

The magnetic field in the equatorial plane can be seen in Fig. 9. The corresponding equatorial plane components of the electric field are zero, notwithstanding the time quadrature. This occurs because the E-field pattern has an odd symmetry with respect to the equatorial plane. Thus, the E-field shown in Fig. 10 has been computed in a plane parallel with the equatorial plane, but displaced by a distance 2.15 mm from the center (close to the resonator face, but still inside the resonator). The meridian plane which contains the maximum electric-field intensity is the $\phi = 0$ plane (Fig. 11), whereas the maximum magnetic-field intensity occurs in the meridian plane $\phi = \pi/2$ (Fig. 12). Note that the magnetic field is very weak outside each resonator face, while the electric field is strongest there. This property should be kept in mind while designing a coupling device for this mode.

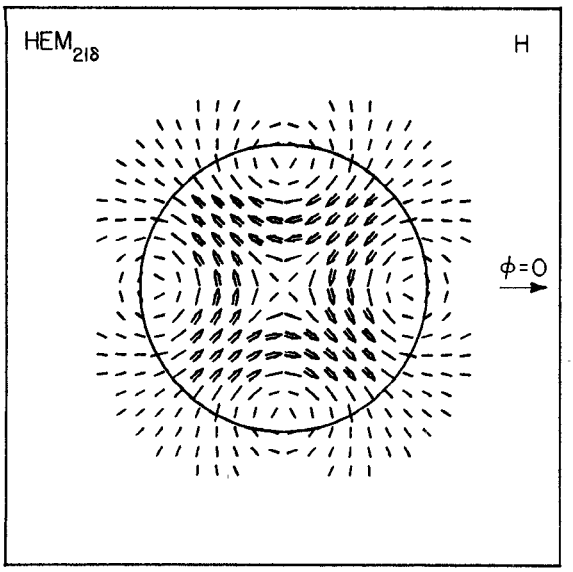

Fig. 16. $HEM_{21\delta}$ mode, H-field in equatorial plane.

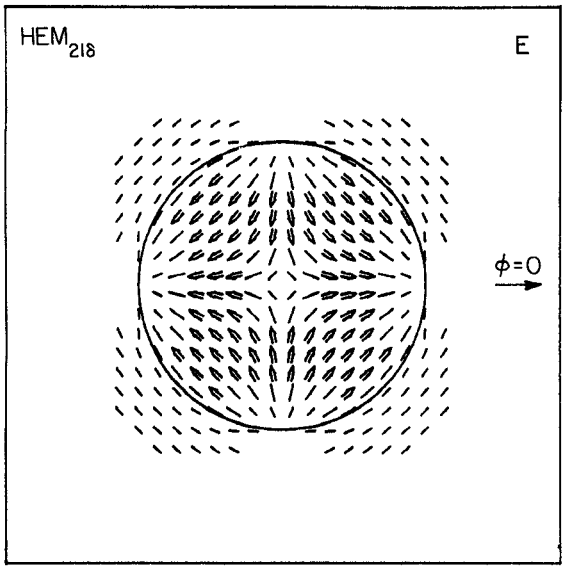

Fig. 17. $HEM_{21\delta}$ mode, E-field in plane parallel to and offset from the equatorial plane by 2.15 mm.

Figs. 13 through 15 depict the mode $HEM_{12\delta}$, which has a resonant frequency only 5 percent higher than the mode $HEM_{11\delta}$ (see Table I). Fig. 13 depicts the electric field in the equatorial plane. In Fig. 14, which shows the E-field in the meridian plane, one notices the strong localized field at the four corners of the resonator. One can expect that, when the resonator is placed face down on a microstrip substrate, this mode will be strongly coupled to the adjacent microstrip line through the electric-field action (capacitive coupling). The magnetic field for this mode in the meridian plane $\phi = \pi/2$ is shown in Fig. 15.

The last four illustrations (Figs. 16 through 19) show the resonant mode $HEM_{21\delta}$. This mode has its resonant frequency close to the resonance of the $TM_{01\delta}$ mode, and if the $TM_{01\delta}$ is the desired mode of operation, $HEM_{21\delta}$ creates a spurious resonance nearby. From Table I one can see that, in the example chosen, the resonant frequencies of

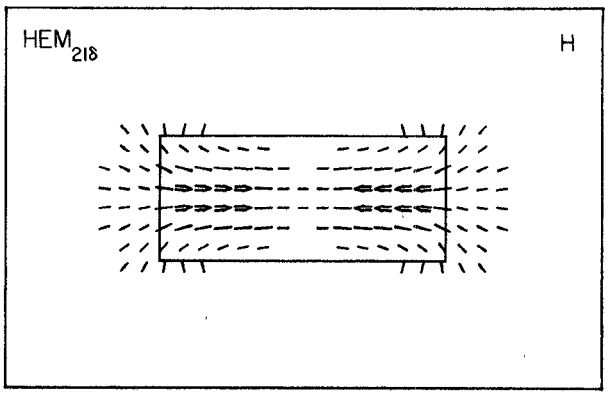

Fig. 18. $HEM_{21\delta}$ mode, H-field in meridian plane $\phi = \pi/4$.

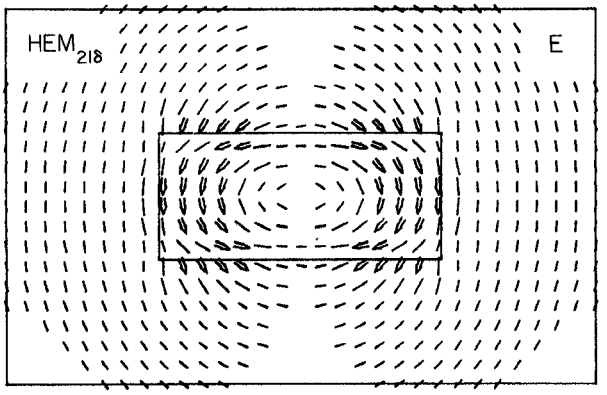

Fig. 19. $HEM_{21\delta}$ mode, E-field in meridian plane $\phi = 0$.

these two modes differ by only 3 percent. Therefore, the field pattern of the $HEM_{21\delta}$ mode is mainly of interest for the purpose of designing an effective mode suppressor. The H-field pattern in the equatorial plane shows an octupole character, consisting of two linear quadrupoles rotated by $\pi/2$ with respect to each other. The octupole is an inefficient radiator, and consequently, the Q factor of this mode is much higher than of any other mode listed in Table I. The electric-field distribution again has an odd symmetry about the equatorial plane. Therefore, the E-field in Fig. 17 is shown close to the surface of the resonator because, at the equatorial plane, the transverse E-field is zero. The H-field in the meridian plane is maximum at $\phi = 45°$. Fig. 18 shows that the magnetic field is strongest near the equator. The E-field in the meridian plane $\phi = 0$ is shown in Fig. 19.

V. Conclusions

The numerical solution of the integral equation for dielectric bodies of revolution provides quantitative and qualitative data of great value for the practical design of dielectric resonators. The circularly symmetric resonant modes ($m = 0$) are classified as $TE_{0n\delta}$ and $TM_{0n\delta}$. The other resonant modes ($m \geq 1$) are all of the hybrid nature, denoted $HEM_{mn\delta}$. The resonant frequencies of various modes are sometimes located very closely together. In order to design the coupling circuits which will enhance the desired resonant mode and suppress the undesirable ones,

a detailed knowledge of the field distribution in the space around the resonator is required. It is hoped that the catalog of the field patterns for the five lowest resonant modes which are presented here will provide users of dielectric resonators with this much needed information.

REFERENCES

[1] A. W. Glisson, D. Kajfez, and J. James, "Evaluation of modes in dielectric resonators using a surface integral equation formulation," *IEEE Trans. Microwave Theory Tech.*, vol. MTT-31, pp. 1023–1029, Dec. 1983.

[2] C. Klein and R. Mittra, "Stability of matrix equations arising in electromagnetics," *IEEE Trans. Antennas Propagat.*, vol. AP-21, pp. 902–905, Nov. 1973.

[3] R. F. Harrington, *Field Computation by Moment Methods*. New York: Macmillan, 1968.

[4] A. J. Poggio and E. K. Miller, "Integral equation solutions of three-dimensional scattering problems," in *Computer Techniques for Electromagnetics*, R. Mittra, Ed. New York: Pergamon, 1973, ch. 3.

[5] J. R. Mautz and R. F. Harrington, "*H*-field, *E*-field and combined-field solutions for conducting bodies of revolution," *Arch. Elek. Übertragung.*, vol. 32, pp. 157–164, Apr. 1978.

[6] J. R. Mautz and R. F. Harrington, "Electromagnetic scattering from a homogeneous material body of revolution," *Arch. Elek. Übertragung.*, vol. 33, pp. 71–80, Feb. 1979.

[7] M. Jaworski and M. W. Pospieszalski, "An accurate solution of the cylindrical dielectric resonator problem," *IEEE Trans. Microwave Theory Tech.*, vol. MTT-27, pp. 639–643, July 1979.

[8] P. Guillon, J. P. Balabaud, and Y. Garault, "TM_{01p} tubular and cylindrical dielectric resonator mode," in *IEEE MTT-S Int. Microwave Symp. Dig.*, June 1981, pp. 163–166.

[9] C. C. Johnson, *Field and Wave Electrodynamics*. New York: McGraw-Hill, 1965.

[10] D. Kajfez, "Basic principles give understanding of dielectric waveguides and resonators," *Microwave Systems News*, vol. 13, pp. 152–161, May 1983.

[11] S. A. Long, M. McAllister, and L. C. Shen, "The resonant cylindrical dielectric cavity antenna," *IEEE Trans. Antennas Propagat.*, vol. AP-31, no. 3, pp. 406–412, May 1983.

✤

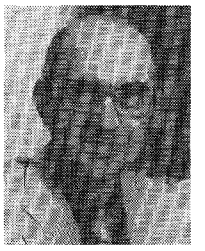

Darko Kajfez (SM'67) was born in Delnice, Yugoslavia, in 1928. He received the Dipl. Ing. degree in electrical engineering from the University of Ljubljana, Yugoslavia, in 1953, and the Ph.D. degree from the University of California, Berkeley, in 1967.

Between 1950 and 1963, he worked with companies "Iskra" and "Rudi Cajavec" in Yugoslavia, primarily in microwave radios and radars. From 1963 to 1966, he was a Research Assistant at the Electronics Research Lab., University of California, Berkeley. In 1967, he joined the University of Mississippi, where he is presently Professor of Electrical Engineering. His research and teaching interests are in electromagnetic theory and its applications to microwave circuits and antennas.

✤

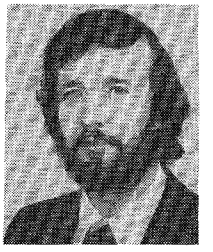

Allen W. Glisson (S'71–M'78) was born in Meridian, MS, on June 26, 1951. He received the B.S., M.S., and Ph.D. degrees in electrical engineering from the University of Mississippi, in 1973, 1975, and 1978, respectively.

From 1973 to 1978, he served as a Research Assistant in the Electrical Engineering Department of the University of Mississippi. In 1978, he joined the faculty of the University of Mississippi, where he is currently Associate Professor of Electrical Engineering. His current research interests include the development and application of numerical techniques for treating electromagnetic radiation and scattering problems.

Dr. Glisson is a member of Sigma Xi, Tau Beta Pi, Phi Kappa Phi, Eta Kappa Nu, and Commission B of the International Union of Radio Science.

✤

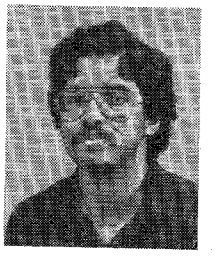

Joseph James (S'84) was born in Chenappady, India, on May 25, 1956. He received the B.S. degree in electronics and communication engineering from the University of Kerala, India, in 1977, and the M.S. degree in electrical engineering from the University of Mississippi in 1984.

From 1978 to 1981, he worked as a Research Engineer with the Electronics Corporation of India Limited, Hyderabad. He is currently with South Carolina State College, Orangeburg, SC.